Viscoelastic Scaling Regimes for Marginally Rigid Fractal Spring Networks

David Head[*]

School of Computing, University of Leeds, Leeds LS2 9JT, United Kingdom

A family of marginally rigid (isostatic) spring networks with fractal structure up to a controllable length was devised, and the viscoelastic spectra $G^*(\omega)$ calculated. Two nontrivial scaling regimes were observed, (i) $G' \approx G'' \propto \omega^\Delta$ at low frequencies, consistent with $\Delta = 1/2$, and (ii) $G' \propto G'' \propto \omega^{\Delta'}$ for intermediate frequencies corresponding to fractal structure, consistent with a theoretical prediction $\Delta' = (\ln 3 - \ln 2)/(\ln 3 + \ln 2)$. The crossover between these two regimes occurred at lower frequencies for larger fractals in a manner suggesting diffusivelike dispersion. Solid gels generated by introducing internal stresses exhibited similar behavior above a low-frequency cutoff, indicating the relevance of these findings to real-world applications.

Introduction.—Many soft matter and complex systems exhibit power-law rheology over a broad frequency range, manifested as parallel scaling of the linear storage and loss moduli $G'(\omega) \propto G''(\omega) \propto \omega^\Delta$ [1–3], or equivalently a power-law relaxation spectrum [4–6]. Relating this scaling to the underlying causal mechanisms would guide the selection of synthesis pathways producing desirable material properties in a number of application domains [7,8], but is not yet generally possible. Of the many potential contributions, slow structural relaxation [9–11] cannot be a prerequisite, as $\Delta \ll 1$ has been observed in protein hydrogels with permanent cross-links and no unfolding [12–14]. There must therefore be processes capable of generating broad distributions of relaxation times that do not require topological changes to material microstructure.

It has been hypothesized that the broad distribution of relaxation times derives from a similarly broad distribution of structural length scales [3,13]. Such structure emerges naturally from cluster aggregation processes, which can produce a scale-invariant, or fractal, geometry up to a characteristic maximum length [15–17]. Calculations for branched fractal polymers predict power-law rheology with a Δ that depends on the fractal dimension d_f and solvent condition [18,19], but cannot explain values $\Delta \ll 1$ without invoking unphysical fractal dimensions [20]. A quite different mechanism applies to tenuous solids close to their rigidity transition, defined here as when $G'(\omega = 0)$ first becomes nonzero, such as at gelation. Normal mode analysis of athermal elastic packings has demonstrated that the lowest eigenvalue, and hence relaxation frequency, vanishes as the rigidity transition is approached, resulting in an arbitrarily broad relaxation spectrum [21–24].

The relative contributions of these two nonexclusive mechanisms to power-law viscoelasticity can be elucidated by the construction and analysis of model systems that are both fractal and marginally rigid. Such systems are considered here. A family of athermal spring networks based on the Sierpinski triangle was devised in which every node connects to $z = 2d = 4$ others, equaling the isostatic threshold when frames first become rigid [25]. These correlated networks [26,27] are fractal up to a controllable length, as in aggregation-derived structures [15–17], and the lower limit of this length produces the kagome lattice [28,29]. These networks are related to those of Machlus *et al.* [30] that however are not locally isostatic everywhere. A matrix-based solver was then used to estimate $G^*(\omega)$ over a broad range of ω, and two nontrivial scaling regimes were found. Low frequencies were consistent with $\Delta = \frac{1}{2}$, also measured for bond-diluted networks, and attributed to marginal rigidity. This matches the exponent for cross-linker-unbinding in semiflexible polymer networks [31] but has a distinct origin. It also matches the intermediate scaling regime for thermal Rouse modes in linear polymers, extended to fractal branched polymers by Muthumukar [18,20], but again a causal relation seems improbable. Conversely, an intermediate frequency regime exhibited $\Delta < \frac{1}{2}$ that was related to the spectral dimension of Sierpinski fractals [32]. The crossover frequency between the two regimes varied with the maximum fractal length in a manner suggesting diffusivelike dispersion. The generalization of these findings to arbitrary fractals are discussed at the end.

Methods.—Arrays of $2^n \times 2^n$ nodes were assembled onto regular triangular lattices with spacing a in a rectangular box of dimensions commensurate to the lattice. The full system was partitioned into two system-spanning triangles with opposite orientations, each with 2^n nodes along each edge. Each triangle was then subdivided into four equal-sized subtriangles with edge length 2^{n-1}, and so on recursively, generating subtriangles with edge lengths

$2^{n-1}\sqrt{3}a$

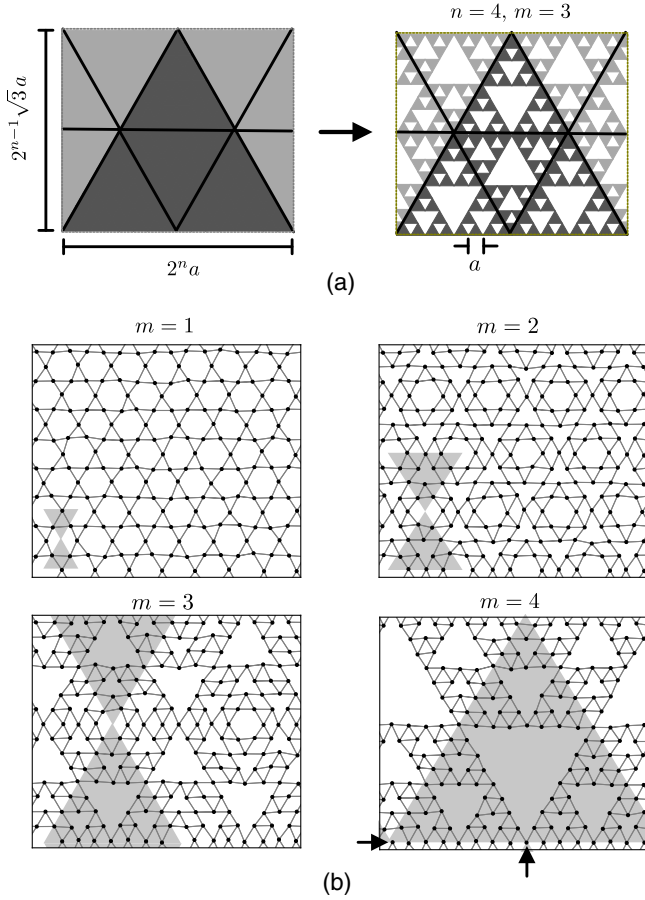$n=4, m=3$

$2^n a$

a

(a)

$m=1$

$m=2$

$m=3$

$m=4$

(b)

FIG. 1. (a) Schematic of network generation for system size $2^n \times 2^n$ and maximum fractal length 2^m. Upward (dark) and downward (light) oriented triangles spanning a periodic box were subdivided into four subtriangles (left). Each subtriangle was then recursively subdivided into three triangles each over $m=3$ further iterations, as per standard Sierpinksi triangles (right). (b) Examples of networks for $n=4$ and $1 \le m \le 4$. Dots denote nodes, and straight lines denote springs. The maximum fractal extent is indicated by the shaded triangles, and the origin has been shifted so all nodes are clearly visible. Arrows indicate the two nodes for $m=n$ with $z=2$. Images for $n=6$ are provided in Ref. [34].

2^{n-2}, 2^{n-3}, etc., for $n-m$ iterations. For the remaining m iterations, only three subtriangles at vertices were recursed as per standard Sierpinski triangle generation, thus generating fractal structure for lengths $2^m a$ down; see Fig. 1(a). Edges of the smallest triangles after the final nth iteration were mapped onto Hookean springs, excluding those lying along the edges of the major triangles with 2^m nodes along each edge. Isolated nodes with no attached springs were removed. To remove colinear springs, x and y coordinates of all nodes were perturbed by small Gaussian displacements with mean zero and variance $(\sigma_j a)^2$, where $\sigma_j = 0.05$. The natural lengths of all springs were set to the internode separation after this perturbation, so there were no internal stresses. When internal stresses were

required, all natural spring lengths were additionally changed by a Gaussian random variable with zero mean and variance $(\Lambda a)^2$, and nodes nonlinearly moved to coordinates obeying static equilibrium using FIRE [33].

Elastic forces on network nodes were required to balance drag forces due to the surrounding fluid throughout cycles of simple oscillatory shear at frequency ω. Hydrodynamic interactions [35,36] were absent; therefore the only degrees of freedom were the complex displacement 2 vectors for each node α, written as $\mathbf{u}^\alpha(t) = \mathbf{u}^\alpha_\omega e^{i\omega t}$ in terms of the complex amplitudes $\mathbf{u}^\alpha_\omega$ (real part understood). The drag force on node α was $\zeta[\mathbf{v}^{\alpha,\text{aff}}(t) - \partial_t \mathbf{u}^\alpha(t)]$ in terms of the drag coefficient ζ and the affine fluid velocity at the position (x^α, y^α) of node α, $\mathbf{v}^{\alpha,\text{aff}}(t) = [\gamma(t)y^\alpha, 0]$ [37]. After canceling all factors of $e^{i\omega t}$, the force balance equations between drag (left-hand side) and elastic (right-hand side) forces were

$$\zeta(\mathbf{v}^{\alpha,\text{aff}}_\omega - i\omega \mathbf{u}^\alpha_\omega) = \sum_{\beta \sim \alpha} H^{\alpha\beta}(\mathbf{u}^\beta_\omega - \mathbf{u}^\alpha_\omega), \quad (1)$$

with $H^{\alpha\beta}$ the 2×2 Hessian matrix for a single spring of stiffness k between connected nodes α and β,

$$H^{\alpha\beta}_{ij} = k\hat{t}^{\alpha\beta}_i \hat{t}^{\alpha\beta}_j + \frac{\tau^{\alpha\beta}}{\ell^{\alpha\beta}}(\delta_{ij} - \hat{t}^{\alpha\beta}_i \hat{t}^{\alpha\beta}_j) \quad (2)$$

in terms of the unit vector $\hat{\mathbf{t}}^{\alpha\beta}$ from α to β, the internode separation $\ell^{\alpha\beta}$, and the spring tension $\tau^{\alpha\beta}$ which vanishes in the absence of internal stresses. Equation (1) was assembled into a global solution vector of all nodal complex amplitudes, and the resulting matrix equation, including Lees–Edwards shifts across sheared boundaries [38], solved using the SuperLU sparse direct method [39] as described previously [36].

Viscoelastic spectra.—Example networks are presented in Fig. 1(b). Every node was connected to $z=4$ others, except for $m=n$, when two nodes in the entire system had $z=2$, resulting from the largest fractal triangles intersecting tip to base through the periodic boundaries, rather than tip to tip as for $m < n$. The kagome lattice [28,29] corresponds to $m=1$, and as $m \to n$, Sierpinksi triangles of fractal dimension $d_f = \ln 3/\ln 2$ [40] became evident. As derived in the Supplemental Material [34], the total number of springs $N_{\text{spring}} = 6(3^m - 2^m)4^{n-m}$ and nodes $N_{\text{node}} = 3(3^m - 2^m)4^{n-m} + \delta_{nm}$, with δ_{nm} the Kronecker delta. Thus the mean coordination number $\langle z \rangle = 2N_{\text{bond}}/N_{\text{node}} = 4$ for $m < n$, with a small correction $4 - \langle z \rangle \sim 4 \cdot 3^{-(m+1)}$ for $m = n$. The pebble game method [41] confirmed all nodes belonged to a single rigid cluster, and there were no redundant springs—that is, springs that can be removed without loss of rigidity—except for a trivial $\mathcal{O}(1)$ set deriving from rigid-body motion of the whole network. This means that all springs become
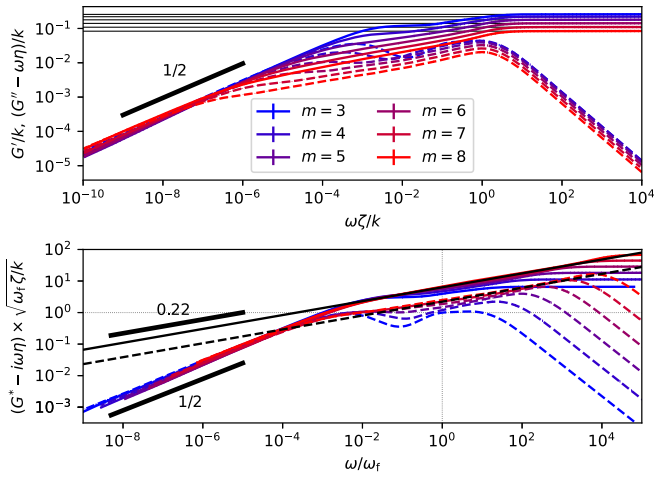
FIG. 2. Viscoelastic spectra for networks of $2^n \times 2^n$ nodes with $n = 10$, with fractal structure up to a length $\propto 2^m$ with m given in the legend. Solid lines denote $G'(\omega)$ scaled to the spring constant k, and dashed lines denote the network contribution (i.e., less the solvent contribution $\eta\omega$ for viscosity η) to $G''(\omega)$. Thin horizontal lines give the affine prediction, $G'_{\mathrm{aff}} = (\sqrt{3}/2)k(3^m - 2^m/4^m)$. The same data is replotted against ω/ω_f with $\omega_f\zeta/k = (2^m)^{-2}$ in the lower panel, with fits to the intermediate scaling regime shown. In both panels, thick line segments have the annotated slope.

stressed, with either positive or negative tension, when the network is sheared.

Viscoelastic spectra $G^*(\omega)$ for different m are given in Fig. 2. It is straightforward to derive the affine prediction $G'_{\mathrm{aff}}/k = (\sqrt{3}/2)(3^m - 2^m/4^m)$ [34], which matches the numerical results for large ω, confirming affinity at frequencies above the highest one-spring mode [42]. By contrast, for low frequencies a power-law scaling $G'(\omega) \approx G''(\omega) \propto \omega^{\Delta}$ with $\Delta \approx 0.5$ was observed. This is consistent with the Kramers–Kronig relation specialized to power-law $G^*(\omega)$, which requires $G''/G' = \tan(\Delta\pi/2)$ [43]. The exponent $\Delta = \frac{1}{2}$ has been predicted by effective medium [37] and scaling [44] theories for nonfractal systems. As the maximum fractal length $\propto 2^m$ was increased, an intermediate frequency regime emerged in which both $G'(\omega)$ and $G''(\omega)$ scaled as a power law $\approx \omega^{\Delta'}$ with $\Delta' \approx 0.22$. The fitted ratio $G''/G' \approx 0.35$ was consistent with the Kramers–Kronig previously mentioned, i.e., $\tan(\Delta'\pi/2) \approx \tan(0.22\pi/2) \approx 0.36$, suggesting this scaling will persist to $\omega \to 0$ for arbitrarily large fractals $2^m \to \infty$. Furthermore, it was possible to collapse curves for $m \geq 3$ onto a single master curve for low and intermediate frequencies by scaling ω by $\omega_f \propto (2^m)^{-2}$, and $G^*(\omega)$ by $(\omega_f)^{1/2}$ so as to preserve $G' \approx G''$ for low ω. Since the maximum fractal length is $\propto 2^m$, this collapse suggests $\omega_f \sim q^2$ for the wavelength $\propto q^{-1} \propto 2^m a$, which is a diffusivelike dispersion relation [1]. The same collapse was also observed for $m = 1, 2$ but to a different master

curve for reasons that are not yet understood; see Fig. S1 of the Supplemental Material [34]. The scaling of the regimes, and the width of the crossovers between them, do not depend on system size as shown in Fig. S2 of the Supplemental Material [34].

$G^*(\omega)$ was also calculated for networks generated by random bond dilution, where springs are present with a probability p. Such networks are known to exhibit a rigidity transition at a critical dilution $p = p_c$ that is well defined for infinite systems [45]. For p sufficiently close to p_c, it was found that the viscoelastic spectra were again consistent with $G'(\omega) = G''(\omega) \propto \omega^{1/2}$, as demonstrated in Fig. S3 of the Supplemental Material [34]. The power-law regime with an exponent ≈ 0.4 previously reported for the lowest frequencies attained by more general numerical schemes [35,37] is also apparent in this figure, and identified here as an intermediate frequency regime.

The exponents for the viscoelastic scaling regimes were confirmed by the scaling framework of Tighe, which, after eliminating a correlation length, predicts $G' \propto G'' \propto \omega^{1-\nu}$, with ν related to the variation of the magnitude of nonaffine displacements, $\mathrm{NA} \propto \sum_\alpha |\mathbf{u}^\alpha - \mathbf{u}^{\alpha,\mathrm{aff}}|^2 \propto \omega^{-\nu}$, where $\mathbf{u}^{\alpha,\mathrm{aff}}$ is the affine displacement for node α [44]. For low frequencies, NA decayed with an exponent $\nu \approx 0.5$ as shown in Fig. S4 of the Supplemental Material [34], consistent with theoretical considerations [46] and the viscoelasticity scaling $\Delta = 1 - \nu = \frac{1}{2}$. For the intermediate frequency regimes, the prediction became $\nu = 1 - \Delta'$, and thus $\nu \approx 1 - 0.22 = 0.78$ for fractal networks and $\approx 1 - 0.4 = 0.6$ for bond-diluted networks, which is again consistent with the NA data in the same figure.

Derivation of Δ'.—Liu recursively generated the dynamical matrix for isolated Sierpinski spring networks to derive the scaling of the density of states [32]. The same approach can be extended to derive a prediction for the slope Δ' of the intermediate regime. Let $F(\tau)$ denote the contribution to rigidity by processes with relaxation time τ, and assume a power-law tail $F(\tau) \sim F_0\tau^{-\mu}$. Following Liu [32], for each additional level of recursion, both the diagonal dynamical matrix elements and the number of degrees of freedom increase by a factor of 3, whereas the effective stiffness halves. For overdamped systems as here, the diagonal scaling suggests an effective damping coefficient that increases threefold, and hence the relaxation time τ—being proportional to damping and inversely proportional to stiffness—increases by a factor of 6. Using τ and τ' to denote relaxation times between successive levels of recursion, this means that

$$\frac{3}{2}F_0(\tau')^{-\mu}d\tau' = F_0\tau^{-\mu}d\tau, \tag{3}$$

with the left-hand side factors 3 for the increase in degrees of freedom, and $\frac{1}{2}$ for the reduction in stiffness. This second factor is absent in Ref. [32]. Inserting $\tau' = 6\tau$ into Eq. (3)

gives $(3/2)6^{1-\mu} = 1$, or $\mu = 2\ln 3/\ln 6$. Using the relation $F(\tau) \propto \tau^{-\mu}$ to $G^*(\omega) \propto \omega^{\mu-1}$ [4,5],

$$\Delta' = \frac{\ln 3 - \ln 2}{\ln 3 + \ln 2} \approx 0.226, \tag{4}$$

in good agreement with the measured value $\Delta' \approx 0.22$.

Internal stresses.—Geometries that sustain states of self-stress can be rigid when networks of the same topology, but with geometries that permit fewer or no states of self-stress, are nonrigid [25,47–49]. Internal stresses were introduced by changing the natural spring lengths by a random amount $\propto \Lambda a$ as described earlier; an example is given in Fig. S5 of the Supplemental Material [34]. As before, application of the pebble game confirmed the lack of redundant bonds for these perturbed geometries, i.e., all springs became either stretched or compressed, as evident from the figure. Viscoelastic spectra varying Λ with m fixed are shown in Fig. 3(a). The spectra for $\Lambda > 0$ match those for $\Lambda = 0$ for high frequencies, changing to a solid response, with constant $G'(\omega)$ and $G''(\omega) \propto \omega$, below a frequency ω_Λ that increases with Λ. Furthermore, it was possible to simultaneously collapse both the low and intermediate frequency regimes for $\Lambda > 0$ by scaling G^* by the plateau modulus $G_0 = G'(\omega = 0)$, and the frequency ω_Λ such that $G''(\omega^*) \propto \omega_\Lambda$ for the lowest frequencies, as shown in Fig. 3(b). The G_0 and ω_Λ used to achieve this collapse are given in Figs. 3(c) and 3(d) respectively, for a range of maximum fractal lengths $\propto 2^m$.

Both the plateau modulus G_0 and the crossover frequency ω_Λ smoothly approach zero as $\Lambda \to 0$, suggesting internal stresses generate rigidity continuously [50] by removing low-frequency response modes. A similar trend was seen for adding random springs, and also for removing springs which induces a crossover to fluidlike (rather than solidlike) response starting at low frequencies, as shown in Fig. S6 of the Supplemental Material [34]. Unlike internal stresses, such perturbations also modify the network connectivity. For $\Lambda \ll 1$, the crossover frequency data are consistent with the quadratic variation $\omega_\Lambda \propto \Lambda^2$ for all m. The variation of G_0 depends upon whether ω_Λ falls in the low- or intermediate-frequency regimes; that is, whether $\omega_\Lambda < \omega_f$ or $\omega_\Lambda > \omega_f$, which in turn is controlled by the fractal length $\propto 2^m$. For small m, $\omega_\Lambda < \omega_f$ for all Λ considered, and $G_0 \propto \Lambda \propto \omega_\Lambda^{1/2}$, consistent with a low-frequency cutoff when $G^* \propto \omega^{1/2}$ scaling is obeyed. Conversely, for larger m when $\omega_\Lambda > \omega_f$ becomes accessible, the data are consistent with $G_0 \propto \Lambda^{2\Delta'} \propto \omega_\Lambda^{\Delta'}$, which itself is consistent with a frequency cutoff in the intermediate regime $G^* \propto \omega^{\Delta'}$. Qualitatively similar results have been observed for elastic sphere packings under compression and elastic beams under shear [48,51], but it is unclear if there is any relationship between the exponents in these systems.
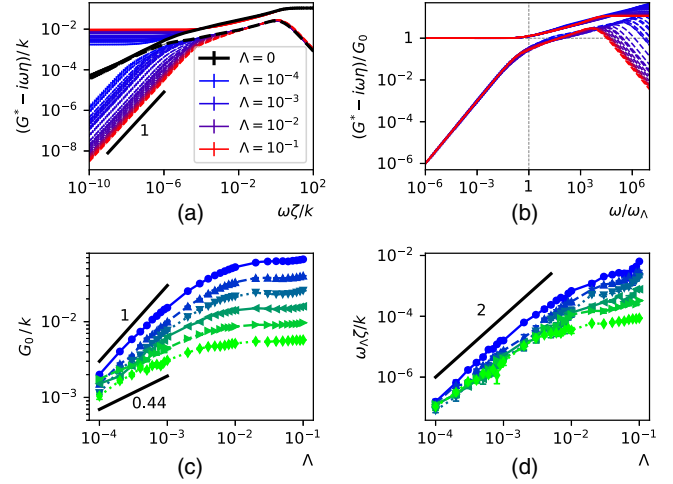

FIG. 3. (a) Viscoelastic spectra for fractal length $\propto 2^m$ with $m = 7$, varying the magnitude of internal stress Λ. The upper set of curves (solid) are G', and the lower (dashed) are the network contribution to G''. Selected values of Λ are given in the legend; curves for other Λ interpolate these. (b) The same data replotted with G^* scaled by $G_0 = G'(\omega = 0)$ and ω scaled by ω_Λ. (c) and (d) give the corresponding values of G_0 and ω_Λ as functions of Λ, increasing incrementally from $m = 3$ (top curves) to $m = 8$ (bottom curves). For all figures, the solid line segments have the annotated slopes.

Discussion.—It has been shown that the design of isostatic networks [52] that are fractal up to an arbitrarily large length is possible, and that for the Sierpinski triangle-based spring networks considered here, power-law viscoelastic scaling was observed with an exponent Δ' that can be theoretically derived. That this scaling survives above a cutoff frequency for systems into the solid phase indicates relevance to real-world applications utilizing postgelled materials. However, a general relation between Δ' and the fractal dimension d_f is not yet available, as existing expressions [18,19] have limited applicability, and the arguments of Liu [32] cannot be easily generalized to arbitrary d_f. The crossover frequency ω_f is not related to a Boson-like peak as this vanishes at isostaticity [22,51]; normal mode analysis might help identify its role in mode propagation. Experimental validation of these trends should be possible by controlling the size of the fractal meso-structure (measured via scattering) varying the volume fraction and/or the reaction rate [12,13]. A broad frequency range at gelation would be accessible using time-cure superposition [53], and should reveal an intermediate power-law regime that is here predicted to extend to lower frequencies for larger fractal lengths. Quantitative agreement would however require the development of three-dimensional models with realistic aggregation kinetics. In addition, any future experimental validation will require quantitative predictions for the crossover frequency between low and intermediate scaling regimes, necessitating three-dimensional modeling. Further work

investigating a broader range of fractal structure with $d = 3$, including dynamically generated stochastic fractals as opposed to the deterministic fractals considered here, would help alleviate these challenges and improve our understanding of the link between fractal structure and viscoelastic response for this important class of materials.

---

[*]d.head@leeds.ac.uk

[1] S. Aime, L. Cipelletti, and L. Ramos, J. Rheol. **62,** 1429 (2018).

[2] J.-T. Hang, Y. Kang, G.-K. Xu, and H. Gao, Nat. Commun. **12,** 6067 (2021).

[3] J. D. J. Rathinaraj, G. H. McKinley, and B. Keshavarz, Fractal Fract. **5,** 174 (2021).

[4] J. E. Martin and D. Adolf, Annu. Rev. Phys. Chem. **42,** 311 (1991).

[5] A. Zaccone, H. H. Winter, M. Siebenbürger, and M. Ballauff, J. Rheol. **58,** 1219 (2014).

[6] L. G. Rizzi, J. Rheol. **64,** 969 (2020).

[7] K. C. Hung, U. S. Jeng, and S. H. Hsu, ACS Macro Lett. **4,** 1056 (2015).

[8] C. Huerta-López and J. Alegre-Cebollada, Nanomater. Nanotechnol. **11,** 1656 (2021).

[9] S. M. Fielding, P. Sollich, and M. E. Cates, J. Rheol. **323,** 323 (1999).

[10] K. Kroy and J. Glaser, New J. Phys. **9,** 416 (2007).

[11] Y. Mulla, F. C. MacKintosh, and G. H. Koenderink, Phys. Rev. Lett. **122,** 218102 (2019).

[12] A. Aufderhorst-Roberts, M. D. G. Hughes, A. Hare, D. A. Head, N. Kapur, D. J. Brockwell, and L. Dougan, Biomacromolecules **21,** 4253 (2020).

[13] M. D. Hughes, B. S. Hanson, S. Cussons, N. Mahmoudi, D. J. Brockwell, and L. Dougan, ACS Nano **15,** 11296 (2021).

[14] A. Aufderhorst-Roberts, D. J. Brockwell, and L. Dougan (to be published).

[15] P. Meakin, Phys. Scr. **46,** 295 (1992).

[16] S. Jungblut, J. O. Joswig, and A. Eychmüller, Phys. Chem. Chem. Phys. **21,** 5723 (2019).

[17] B. S. Hanson and L. Dougan, Macromolecules **53,** 7335 (2020).

[18] M. Muthukumar, J. Chem. Phys. **83,** 3161 (1985).

[19] J. E. Martin, D. Adolf, and J. P. Wilcoxon, Phys. Rev. A **39,** 1325 (1989).

[20] M. Muthukumar, Macromolecules **22,** 4656 (1989).

[21] A. Lemaître and C. Maloney, J. Stat. Phys. **123,** 415 (2006).

[22] L. E. Silbert, A. J. Liu, and S. R. Nagel, Phys. Rev. E **79,** 021308 (2009).

[23] E. M. Huisman and T. C. Lubensky, Phys. Rev. Lett. **106,** 088301 (2011).

[24] R. Milkus and A. Zaccone, Phys. Rev. E **95,** 023001 (2017).

[25] C. R. Calladine, Int. J. Solids Struct. **14,** 161 (1978).

[26] J. Michel and P. Yunker, Proc. Natl. Acad. Sci. U.S.A. **116,** 2875 (2019).

[27] S. Zhang, L. Zhang, M. Bouzid, D. Z. Rocklin, E. DelGado, and X. Mao, Phys. Rev. Lett. **123,** 058001 (2019).

[28] K. Sun, A. Souslov, X. Mao, and T. C. Lubensky, Proc. Natl. Acad. Sci. U.S.A. **109,** 12369 (2012).

[29] X. Mao, O. Stenull, and T. C. Lubensky, Phys. Rev. E **87,** 042602 (2013).

[30] S. Machlus, S. Zhang, and X. Mao, Phys. Rev. E **103,** 012104 (2021).

[31] C. P. Broedersz, M. Depken, N. Y. Yao, M. R. Pollak, D. A. Weitz, and F. C. MacKintosh, Phys. Rev. Lett. **105,** 238101 (2010).

[32] S. H. Liu, Phys. Rev. B **30,** 4045 (1984).

[33] E. Bitzek, P. Koskinen, F. Gahler, M. Moseler, and P. Gumbsch, Phys. Rev. Lett. **97,** 170201 (2006).

[34] See Supplemental Material at http://link.aps.org/supplemental/10.1103/PhysRevLett.129.018001 for additional calculations and figures.

[35] M. Dennison and H. Stark, Phys. Rev. E **93,** 022605 (2016).

[36] D. Head and C. Storm, Phys. Rev. Lett. **123,** 238005 (2019).

[37] M. G. Yucht, M. Sheinman, and C. P. Broedersz, Soft Matter **9,** 7000 (2013).

[38] M. P. Allen and D. J. Tildesley, *Computer Simulations of Liquids* (Clarendon Press, Oxford, 1987).

[39] J. W. Demmel, S. C. Eisenstat, J. R. Gilbert, X. S. Li, and J. W. H. Liu, SIAM J. Matrix Anal. Appl. **20,** 720 (1999).

[40] K. Falconer, *Fractal Geometry: Mathematical Foundations and Applications*, 3rd ed. (Wiley, New York, 2014).

[41] D. J. Jacobs and M. F. Thorpe, Phys. Rev. Lett. **75,** 4051 (1995).

[42] E. M. Huisman, C. Storm, and G. T. Barkema, Phys. Rev. E **82,** 061902 (2010).

[43] F. Chambon and H. H. Winter, J. Rheol. **31,** 683 (1987).

[44] B. P. Tighe, Phys. Rev. Lett. **109,** 168303 (2012).

[45] M. Sahimi, *Heterogeneous Materials I: Linear Transport and Optical Properties* (Springer-Verlag, New York, 2003).

[46] M. Wyart, H. Liang, A. Kabla, and L. Mahadevan, Phys. Rev. Lett. **101,** 215501 (2008).

[47] S. Pellegrino and C. R. Calladine, Int. J. Solids Struct. **22,** 409 (1986).

[48] M. F. J. Vermeulen, A. Bose, C. Storm, and W. G. Ellenbroek, Phys. Rev. E **96,** 053003 (2017).

[49] A. Bose, M. F. J. Vermeulen, C. Storm, and W. G. Ellenbroek, Phys. Rev. E **99,** 023001 (2019).

[50] M. Merkel, K. Baumgarten, B. P. Tighe, and M. L. Manning, Proc. Natl. Acad. Sci. U.S.A. **116,** 6560 (2019).

[51] M. Wyart, L. E. Silbert, S. R. Nagel, and T. A. Witten, Phys. Rev. E **72,** 051306 (2005).

[52] M. Sadjadi, V. F. Hagh, M. Kang, M. Sitharam, R. Connelly, S. J. Gortler, L. Theran, M. Holmes-Cerfon, and M. F. Thorpe, Phys. Status Solidi (b) **258,** 2000555 (2021).

[53] D. Adolf and J. E. Martin, Macromolecules **23,** 3700 (1990).